Progress In Electromagnetics Research, PIER 20, 213–226, 1998

FIELDS IN THE FOCAL SPACE OF SYMMETRICAL HYPERBOLIC FOCUSING LENS

W. B. Dou, Z. L. Sun, and X. Q. Tan

State Key Lab of Millimeter Waves
Dept. of Radio Engr., Southeast University
Nanjing, 210096, P.R. China

1. INTRODUCTION

The knowledge of focal region field of focusing element, such as parabolic antennas and lens, is useful for synthesizing feed arrays in imaging and design of multiple beam antenna. Many investigations on the fields in focal space of parabolic reflector antenna have been carried out [1–3]. Millimeter wave imaging now attracts more attentions. One approach is focal plane imaging system. Focal plane array technology has been adopted as design approach for imaging systems in the 2 mm to 3 mm wavelength range [4]. However, the limited volume available restricts f/D for lens systems to values ≤ 1.25, which seriously restricts imaging capability. To evaluate the imaging performance it is necessary to get the field distribution in the focal space of a focusing lens. It is useful for selecting the feed element, evaluating the packing efficiency and coupling between lens and feed element. The usual optical analysis of the focal region is inadequate for investigating this possibility. Airy's well-known equation $2J_1(u)/u$, for the amplitude distribution in the focal plane of a circular lens, is valid only for the large focal ratios f/D common in optical systems. Although both am-

plitude and phase near the focus of a lens have been studied at both optical and microwave frequencies [5–6], the scalar-wave theory used gives no information on the detailed configuration of the electromagnetic fields in the image. A vector solution is therefore sought for the fields in the focal region of a lens. It is just the purpose of this paper.

2. ANALYSIS

The configuration to be analyzed is shown in Fig. 1. A linearly polarized wave is incident obliquely on the surface S_1 of the lens. It is assumed that the polarization of incident wave is in $X-Z$ plane. If the polarization is in $Y-Z$ plane, similar results also can be obtained. Thus incident wave is given by

$$\vec{E}_i = (\hat{x}\cos\theta_0 - \hat{z}\sin\theta_0)\cdot\exp(jk(x\sin\theta_0 + z\cos\theta_0)) \tag{1}$$

Using the ray tracing techniques the fields on surface S_2 can be gotten. Then the field in the focal space can be calculated by using following diffraction integration [7]

$$\vec{E}_p = \frac{i}{4\pi\omega\varepsilon}\int_s \Big[(\vec{J}\cdot\nabla)\nabla + k^2\vec{J} - j\omega\varepsilon\vec{J}_m\times\nabla\Big]\frac{\exp(-jkr_s)}{r_s}ds \tag{2}$$

$$\vec{J} = \vec{n}\times\vec{H}, \qquad \vec{J}_m = -\vec{n}\times\vec{E} \tag{3}$$

where r_s is the distance between source point and field point, $\vec{H}$ and $\vec{E}$ are the fields on the surface S_2. From equation (2) following equations can be deduced.

$$\vec{E}_p = \vec{E}_{p1} + \vec{E}_{p2} + \vec{E}_{p3} \tag{4}$$

$$\vec{E}_{p1} = -j\frac{k^2}{4\pi\omega\varepsilon}\int_s \Big[-(\vec{J}\cdot\hat{r}_s)\hat{r}_s + \vec{J} + \sqrt{\frac{\varepsilon}{\mu}}\vec{J}\times\hat{r}_s\Big]\frac{\exp(-jkr_s)}{r_s}ds \tag{5}$$

$$\vec{E}_{p2} = -j^2\frac{k^2}{4\pi\omega\varepsilon}\int_s \Big[(\vec{J}\cdot\hat{r}_s)\hat{r}_s\frac{3}{r_s} - \frac{\vec{J}}{r_s} - \frac{1}{r_s}\sqrt{\frac{\varepsilon}{\mu}}\vec{J}\times\hat{r}_s\Big]\frac{\exp(-jkr_s)}{r_s}ds \tag{6}$$

$$\vec{E}_{p3} = -\frac{j}{4\pi\omega\varepsilon}\int_s \Big[(\vec{J}\cdot\hat{r}_s)\hat{r}_s\frac{1}{r_s^2} - \frac{\vec{J}}{r_s^2}\Big]\frac{\exp(-jkr_s)}{r_s}ds \tag{7}$$

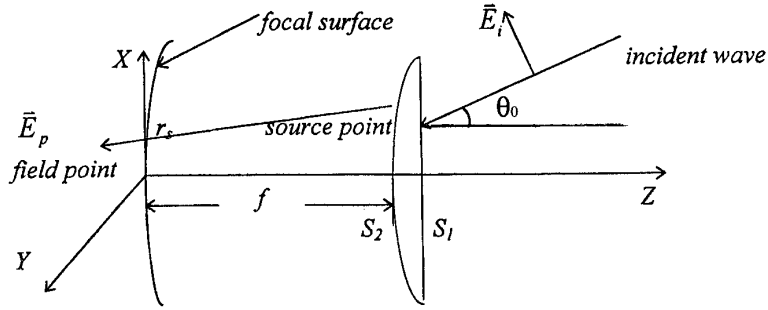

Figure 1. Geometry of symmetric focusing lens.

where $\hat{r}_s$ is the unit vector from source point to field point.

$\vec{E}_{p3}$ is small compared to the $\vec{E}_{p1}$ and $\vec{E}_{p1}$, so it is neglected. Vectorial equations (5) and (6) can be decomposed to three scalar equations for E_x, E_y and E_z, respectively. Then integration surface is divided to many small areas, doing integration numerically to each area and adding up all the contributions of every area the fields in focal region can be obtained. Fields in focal surface are also considered besides that in focal plane, $X - Y$ plane.

The coupling η_c between the focusing lens and a horn on focal plane is defined by

$$\eta_c = \eta_p \cdot \eta \tag{8}$$

where η_p is the ratio of the power P_A in Airy pattern and the power P_i received by the lens

$$\eta_p = \frac{P_A}{P_i} \tag{9}$$

η is the coupling efficiency between the field of Airy pattern and the field in aperture of the horn. It is defined as

$$\eta = \frac{\left| \int\limits_s \vec{E}_w \cdot \vec{E}_f^* ds \right|^2}{\int\limits_s |\vec{E}_w|^2 ds \int\limits_s |\vec{E}_f|^2 ds} \tag{10}$$

where integration region S is the region having same area occupied by Airy pattern at center of focal plane and the center of S coincides with the peak of Airy pattern. $\vec{E}_w$ is the field in the aperture of the horn with the same radius as that of Airy pattern at center of focal

plane. $\vec{E}_f$ is the field of Airy pattern. $*$ denotes conjugate complex quantity.

3. CALCULATION RESULTS

In Fig. 2, the image structure (we also call it Airy pattern from now on) calculated here when the wave is incident normally for different focal ratio f/D are compared with the classical Airy pattern, deduced by scalar analysis, of optical focusing systems. The calculation parameters are: lens radius $R_0 = 100$ mm; focal length $f = 200$ mm, 260 mm, 350 mm, respectively; dielectric constant of the hyperbolic lens $\varepsilon_r = 2.54$; frequency of incident wave $f_0 = 94$ GHz; The solid line is the classical Airy pattern, dash line is calculated results here. The calculated image structures are different to some extent from the classical Airy pattern. Its shape is wider than the Airy pattern and gradually approaches the Airy pattern with f/D increasing.

From calculations it also can be seen that the fields in the axial region of focal plane approximate to the field in the aperture of a corrugated horn with the same radius as that of Airy pattern, under balanced hybrid condition [8]. Fig. 3 shows the comparison.

In Fig. 4 the three dimensional field structures and their contour curves are shown. When the oblique angle of incident wave is increased, the field structure is distorted gradually due to the phase errors or aberrations. Each field structure is normalized to its maximum amplitude.

To show the vectorial characteristic of the field in focal plane, Table 1 gives the ratio of E_{ymax}/E_{xmax} and E_{zmax}/E_{xmax} for different incident angle θ_0. E_x is copolarized field, E_y is cross-polarized field for situation here. $E_{xmax}(\theta_0)/E_{xmax}(0)$, which displays the effect of the aberration on Airy pattern, is also given in Table 1. In Fig. 3, Fig. 4 and Table 1 the lens radius $R_0 = 100$ mm; focal length $f = 260$ mm; dielectric constant of the lens $\varepsilon_r = 2.54$; frequency of incident wave $f_0 = 94$ GHz;

	$\theta_0 = 0°$	$\theta_0 = 1°$	$\theta_0 = 2°$	$\theta_0 = 3°$	$\theta_0 = 4°$
$E_{xmax}(\theta_0)/E_{xmax}(0)$	1	0.9738	0.8924	0.7635	0.6335
E_{ymax}/E_{xmax}	0.0	0.0	0.0	0.0	0.0
E_{zmax}/E_{xmax}	0.02	0.03	0.06	0.07	0.07

Table 1

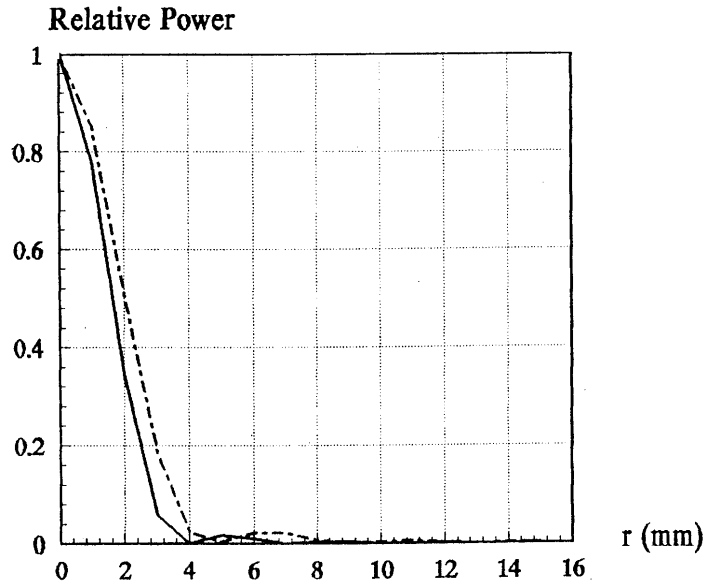

2a. Focal length $f = 200\,\text{mm}$, $f/D = 1.0$.

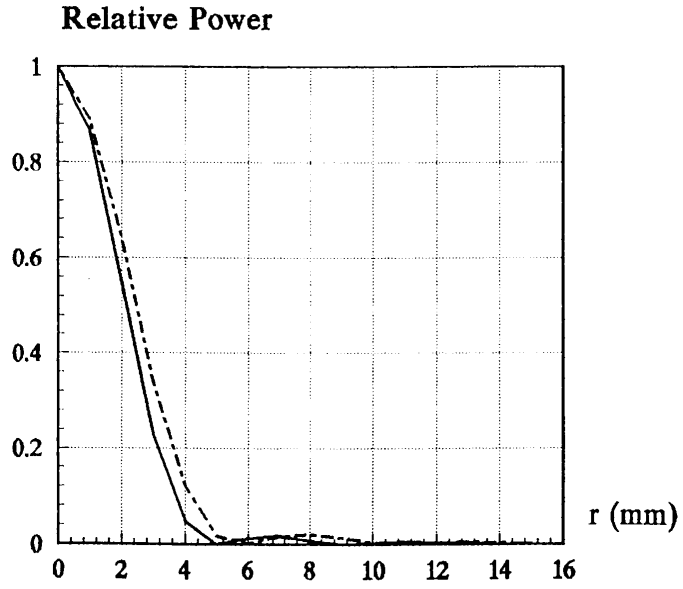

2b. Focal length $f = 260\,\text{mm}$, $f/D = 1.3$.

Figure 2. The comparison between calculated image structures and classical Airy pattern

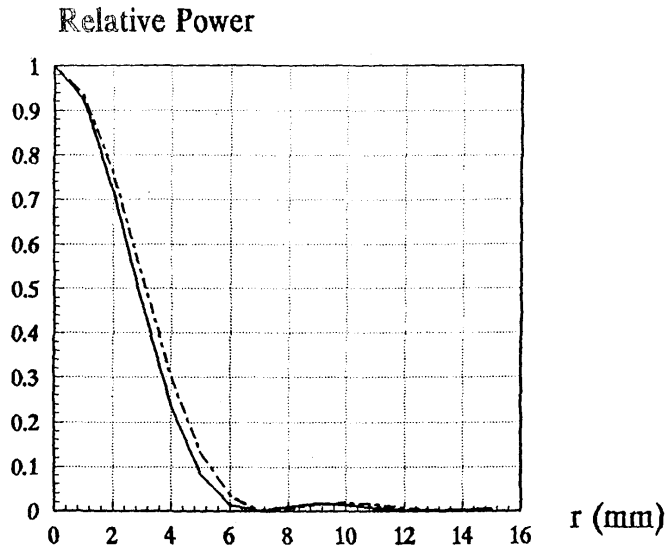

2c. Focal length $f = 350\,\text{mm}$, $f/D = 1.75$.

Figure 2. The comparison between calculated image structures and classical Airy pattern

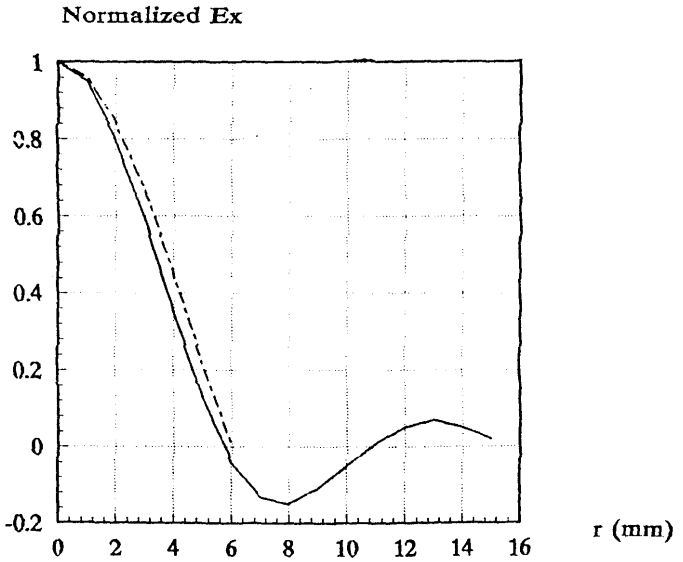

Figure 3. The fields comparison dash line-field in the aperture of horn; solid line-field in the axial region of focal plane.

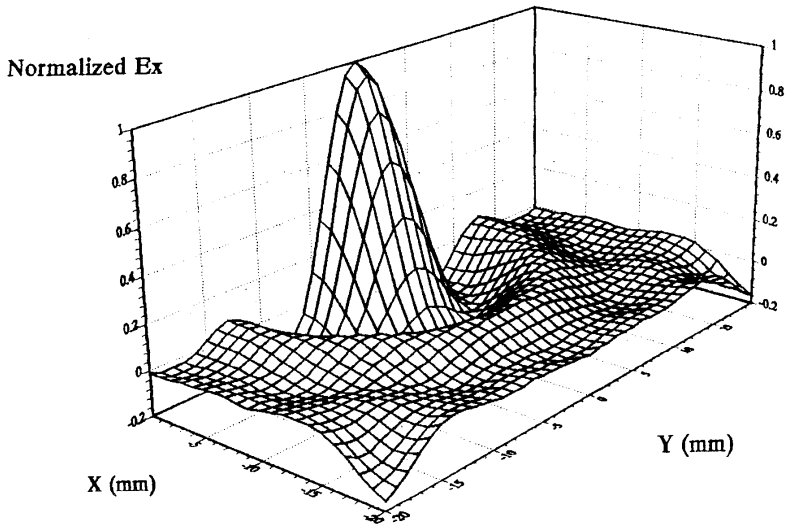

3 dimensional diagram

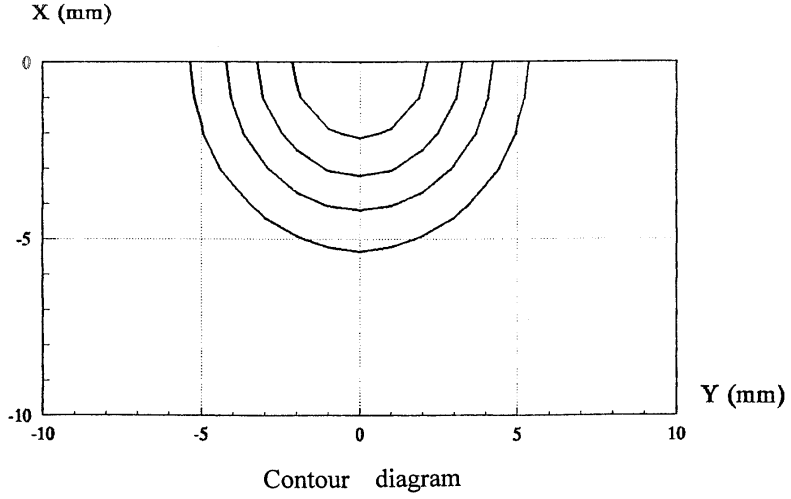

(a) Oblique angle $\theta_0 = 0°$.

Figure 4. Field structure in focal plane for different oblique angle of incident wave.

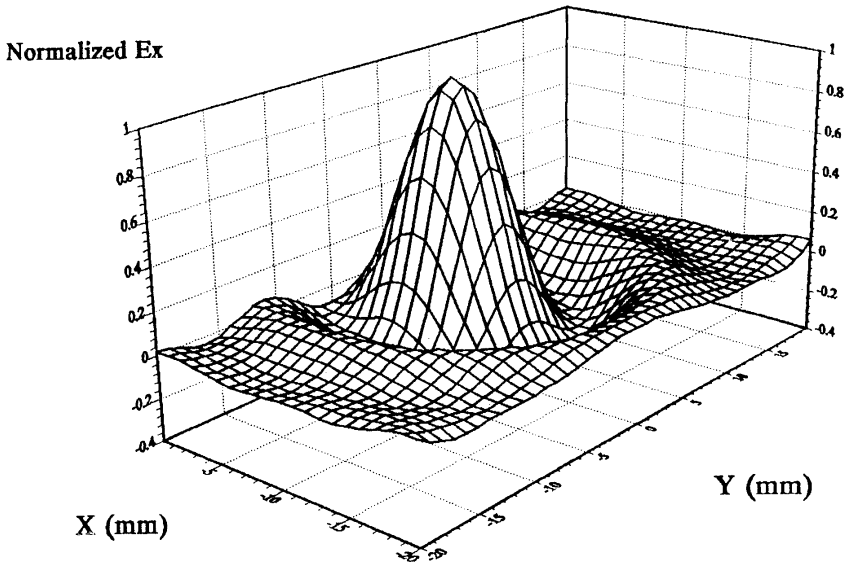

3 dimensional diagram

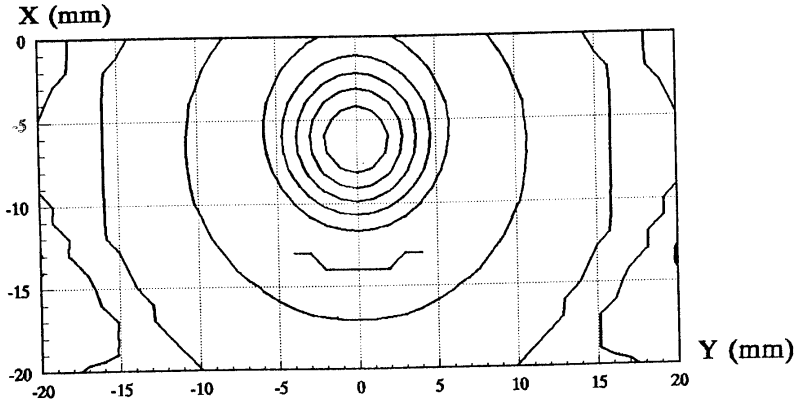

Contour diagram

(b) Oblique angle $\theta_0 = 1^\circ$.

Figure 4. Field structure in focal plane for different oblique angle of incident wave.

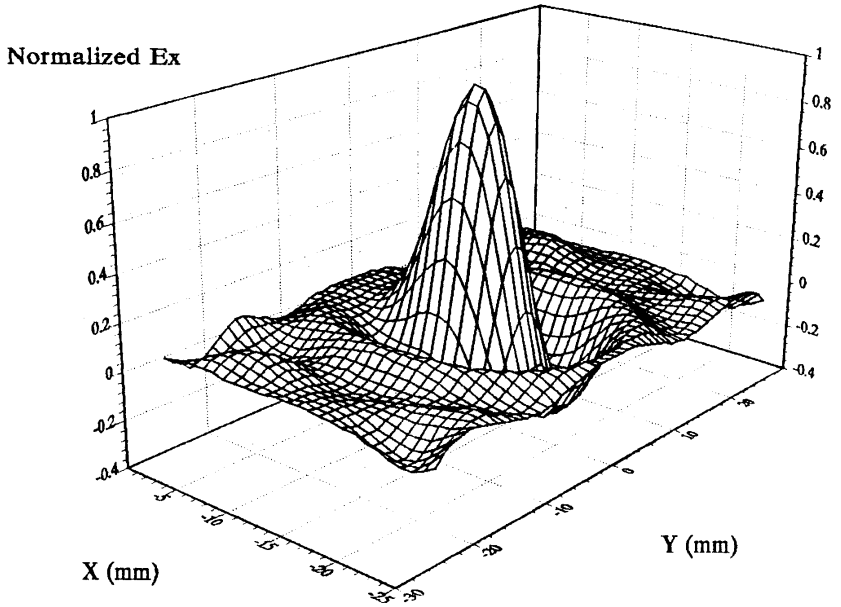

3 dimensional diagram

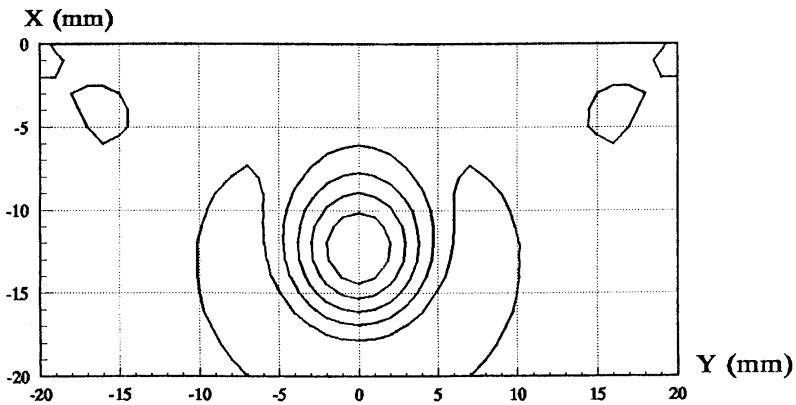

Contour diagram

(c) Oblique angle $\theta_0 = 2°$.

Figure 4. Field structure in focal plane for different oblique angle of incident wave.

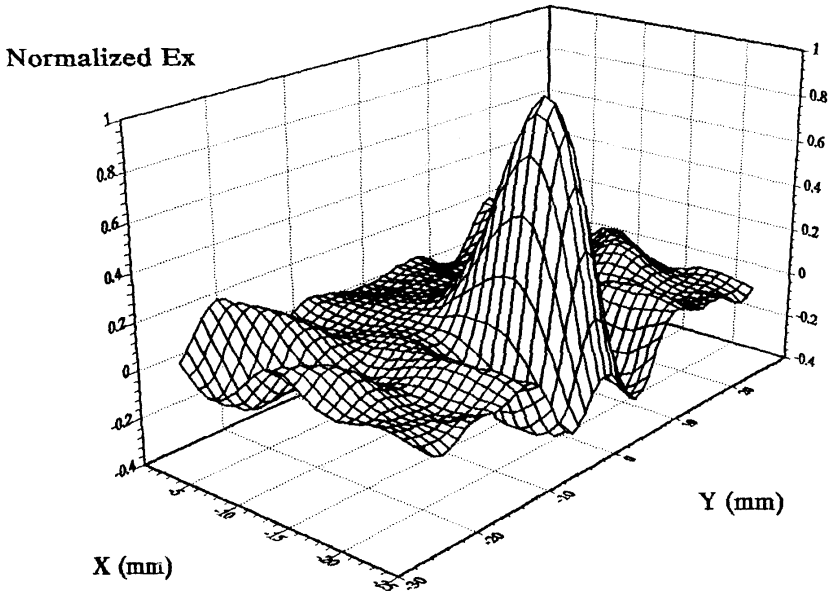

3 dimensional diagram

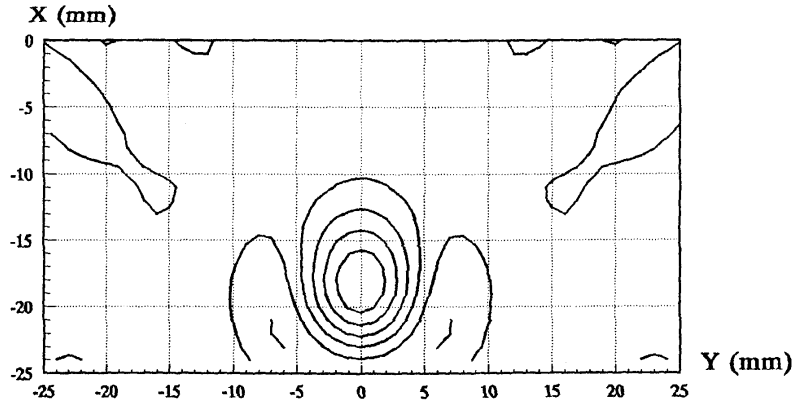

Contour diagram

(d) Oblique angle $\theta_0 = 3°$.

Figure 4. Field structure in focal plane for different oblique angle of incident wave.

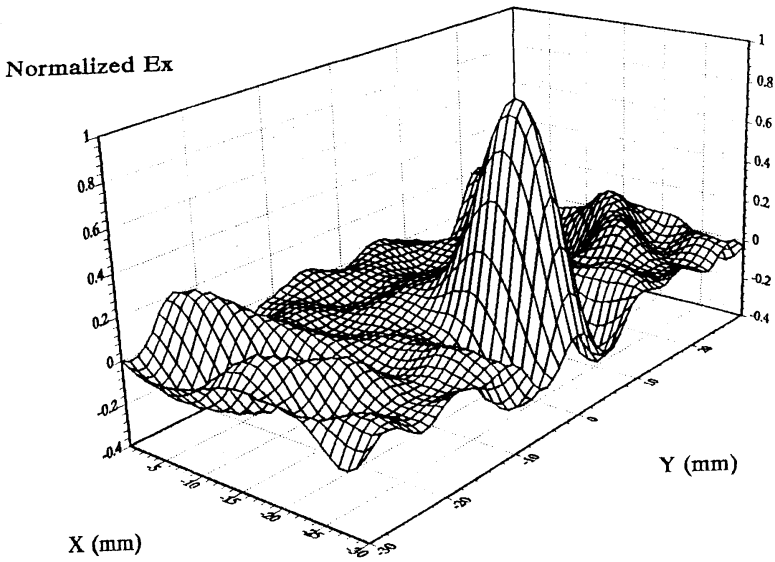

3 dimensional diagram

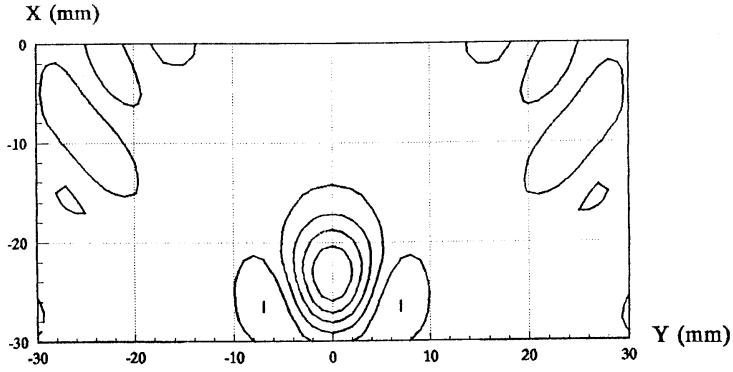

Contour diagram

(e) Oblique angle $\theta_0 = 4^\circ$.

Figure 4. Field structure in focal plane for different oblique angle of incident wave.

For the focal ration f/D considered here, E_y and E_z are small compared to the E_x.

The coupling between the focusing lens and a horn on focal plane is given in Table 2 for the same lens.

	$\theta_0 = 0^\circ$	$\theta_0 = 1^\circ$	$\theta_0 = 2^\circ$	$\theta_0 = 3^\circ$	$\theta_0 = 4^\circ$
η_p	0.7928	0.7312	0.6355	0.5119	0.3927
η	0.9961	0.9728	0.9631	0.9618	0.8905
η_c	0.7897	0.7113	0.6120	0.4923	0.3496

Table 2

Another important property interested is resolution of the lens. In the absence of aberrations each point object would, according to geometrical optics, give rise to a sharp point image. Because of diffraction the actual image will nevertheless always be a finite patch of light. And if two such image patches (diffraction patterns) overlap, it will be more and more difficult to detect the presence of two objects, the closer the central intensity maximums are to each other. Nevertheless it is desirable to have some simple criterion which permits a rough comparison of the relative efficiency of different systems, and for this purpose Rayleigh's criterion may be employed. According to this criterion two images are regarded as just resolved when the two image patch overlap at 0.7 of their principal maximum.

In Fig. 5 the resolution ability of the lens is displayed. In the region of radius less 15 mm the angle resolution is 0.8°, beyond this region angle resolution is degraded gradually.

The field distribution in a focal surface whose radius is 270 mm is also calculated to see if the angle resolution is improved. Unfortunately, no improvement has been realized.

It can be seen from calculations:

1. The fields in the axial region of focal plane approximate to the fields in the aperture of corrugated horn under balanced hybrid condition.
2. The calculated image structures are different to some extent from the classical Airy pattern. Its shape is wider than the Airy pattern and gradually approaches the Airy pattern with f/D increasing.
3. When the oblique angle of incident wave is increased, the imaging resolution and the coupling between lens and corrugated horn are decreased because of the distortion of the field structure in focal plane.

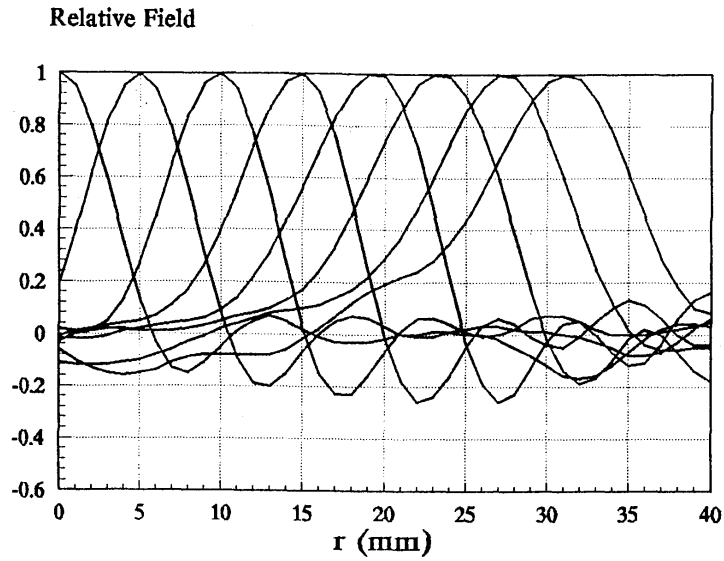

Figure 5. The calculated angle resolution of the lens in focal plane. The incident angle is stepped by $\delta\theta = 0.8°$

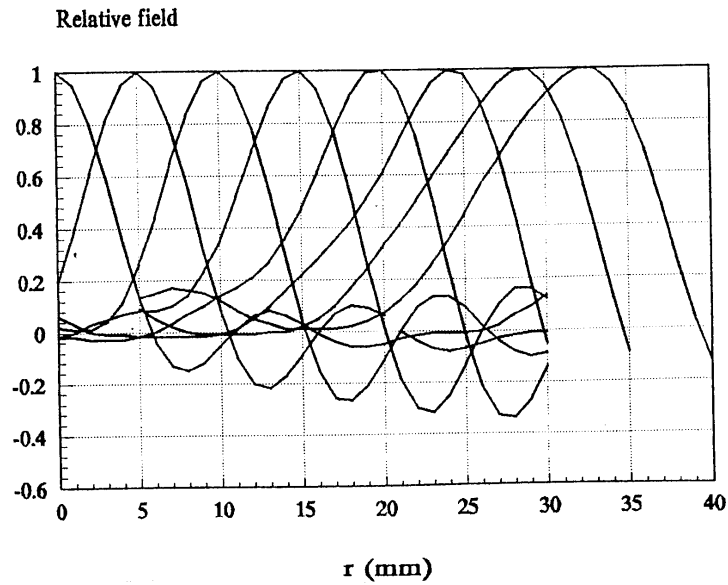

Figure 6. The calculated angle resolution of the lens in focal surface. The incident angle is stepped by $\delta\theta = 0.8°$.

4. For the considered situation here, E_y and E_z are small compared to the copolarized field E_x.

4. CONCLUSION

The fields distribution in the focal space of a symmetrical hyperbolic lens is calculated by a well-known electromagnetic field formula. They provide much information which is useful for selecting the feed element, evaluating the packing efficiency and coupling between lens and feed element in focal plane imaging. It is also useful for multibeam antenna design in communication systems.

REFERENCES

1. Nagamune, A., and P. H. Pathak, "An efficient plane wave spectral analysis to predict the focal region fields of parabolic reflector antennas for small and wide angle scanning," *IEEE Trans. AP*, Vol. 38, No. 11, 1746–1756. 1990,
2. Minnett, H. C., and B. M. Thamos, "Fields in the image space of symmetrical focusing reflectors," *Proc. IEE*, Vol. 115, No. 10, 1419–1430, 1968.
3. Watson, W. H., "The field distribution in the focal plane of a Paraboloidal Reflector," *IEEE Trans. AP*, Vol. 12, 561–569, Sept. 1964.
4. Goldsmith, P. F., et al., "Focal plane imaging systems for millimeter wavelength," *IEEE Trans. MTT*, Vol. 41, No. 10, 1664–1676, 1993.
5. Rubin, W. L., and J. V. DiFranco, "A high resolution interferometer radar with low angle ambiguity," *IRE Trans. AP*, Vol. 11, 197–198, ,1963.
6. Dausin, L. R., et al., "The effects of wide band signals on radar antenna design," *IRE WESCON Convention Record*, pt. 1, 40–45, 1959.
7. Silver, S., "Microwave Antenna Theory and Design," *IEE Series on Electromagnetic Waves*, No. 19, 1984.
8. Wylde, R. J., "Milimeter-Wave Gaussian beam-made optics and corrugated feed horns," *IEE Proc. H*, Vol. 131, No. 4, 258–262, 1984.